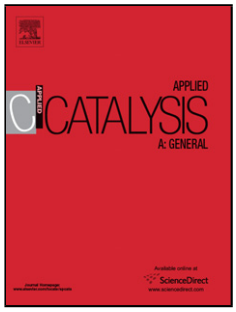

Title: Water-Enhanced Selective Hydrogenation of Cinnamaldehyde to Cinnamyl Alcohol on RuSnB/CeO_2 Catalysts

Authors: Yihu Dai, Xiaofang Chu, Jingjing Gu, Xing Gao, Min Xu, Di Lu, Xiaoyue Wan, Wei Qi, Bingsen Zhang, Yanhui Yang

PII: S0926-860X(19)30245-5
DOI: https://doi.org/10.1016/j.apcata.2019.05.032
Reference: APCATA 17098

To appear in: *Applied Catalysis A: General*

Received date: 8 April 2019
Revised date: 26 May 2019
Accepted date: 28 May 2019

Please cite this article as: Dai Y, Chu X, Gu J, Gao X, Xu M, Lu D, Wan X, Qi W, Zhang B, Yang Y, Water-Enhanced Selective Hydrogenation of Cinnamaldehyde to Cinnamyl Alcohol on RuSnB/CeO_2 Catalysts, *Applied Catalysis A, General* (2019), https://doi.org/10.1016/j.apcata.2019.05.032

Water-Enhanced Selective Hydrogenation of Cinnamaldehyde to Cinnamyl Alcohol on RuSnB/CeO_2 Catalysts

Yihu Dai[a,*], Xiaofang Chu[a], Jingjing Gu[a], Xing Gao[a], Min Xu[a], Di Lu[a], Xiaoyue Wan[a], Wei Qi[b,*], Bingsen Zhang[b], Yanhui Yang[a,*]

[a]Institute of Advanced Synthesis, School of Chemistry and Molecular Engineering, Nanjing Tech University, Nanjing 211816, China

[b]Shenyang National Laboratory for Materials Science, Institute of Metal Research, Chinese Academy of Sciences, Shenyang 110016, China

Corresponding Author

*E-mail: ias_yhdai@njtech.edu.cn (Y. Dai)

*E-mail: wqi@imr.ac.cn (W. Qi)

*E-mail: yhyang@njtech.edu.cn (Y. Yang)

Highlights:

- RuSnB/CeO_2 efficiently catalyzes cinnamaldehyde

hydrogenation to cinnamyl alcohol in water.

- Structural and electronic modification by Sn and B species enhance catalytic property of Ru sites.
- Water-involved hydrogen-exchange route co-exists with H_2-dissociation-hydrogenation.
- H_2-dissociation is not rate-limiting step whereas facile H_2O-activation accelerates reaction.

Abstract: The CeO_2-supported ternary RuSnB catalysts were synthesized by incipient wetness impregnation procedures and applied in hydrogenation of cinnamaldehyde in pure water as the solvent. A synergy effect between Ru-based catalysts and water molecules has afforded the efficiently selective transformation of cinnamaldehyde to cinnamyl alcohol with the satisfactory conversion and selectivity. Structural characterization results suggested the incorporation of Ru sites into the SnO_x matrix and the electronic interaction between Ru and B additives in $RuSnB/CeO_2$ catalyst. The isotopic exchange studies have demonstrated that both dissociative activation of H_2 and H_2O (deuterated D_2 and D_2O) were apparently affected by the status of Ru sites. Furthermore, the kinetics tests in D_2O solvent have also revealed the co-existence of water-involved hydrogen-exchange route with the direct hydrogenation route using dissociative H_2 during the hydrogenation reaction. The optimal

$Ru_2Sn_1B_1/CeO_2$ catalyst could afford the best H_2O-activation capability and thus accelerate the reaction rate in the H_2O-involved hydrogenation.

Keywords: water, Ru catalyst, hydrogen exchange, selective hydrogenation, α,β-unsaturated aldehyde and alcohol

1. Introduction

A wide variety of α,β-unsaturated alcohols serve as important fine chemicals applied in agrochemicals, flavorings, pharmaceuticals, fragrances industrials, and these alcohols can be manufactured through the chemoselective hydrogenation of the carbonyls in α,β-unsaturated aldehydes and ketones [1-4]. Although such reaction route has a high degree of atom-economy, it is still subject to the issue of unsatisfactory hydrogenation selectivity, because C=C bonds possess lower bond energy than C=O bonds and both thermodynamics and kinetics favor the activating hydrogenation of C=C bonds over C=O bonds [5,6]. Different kinds of heterogeneous metallic catalysts have been developed to accomplish the selective hydrogenation of α,β-unsaturated aldehydes and ketones to corresponding unsaturated alcohols through the structural optimization on active metal sites and supports as well as ligands [7-14]. With respect to focused researches of the precious metal catalysts, Pd catalysts prefer to selectively catalyze hydrogenation of C=C moiety over C=O moiety, causing the formation of C=C hydrogenated products [15]. On the other hand, the high-cost limits

the practical application of Ir and Pt catalysts in the hydrogenation of α,β-unsaturated aldehydes and ketones, although numerous optimization efforts have been successful [16-22]. In consideration of affordable price and moderate catalytic hydrogenation ability, metallic Ru heterogeneous catalysts have potentials to meet the challenges of efficiently selective transformation of α,β-unsaturated aldehydes and ketones into α,β-unsaturated alcohols.

There are various attempts to enhance the performance of Ru-based catalysts in selective hydrogenation reactions of α,β-unsaturated aldehydes and ketones. Moderate size distribution and high dispersion degree of metallic Ru nanoparticles on the catalyst surfaces is necessary to increase the catalytic activity, however, excessively small particle size leads to decreased hydrogenation selectivity towards the unsaturated alcohols [23,24]. Introducing a second metal additive to form alloy structure has also been proved as a feasible strategy to improve both catalytic hydrogenation activity and selectivity for Ru-based catalysts [25,26]. Benefited to electronic effects and geometric effects, satisfactory catalytic property can be gained on those bimetallic alloy Ru-series catalysts, e.g., Ru-Fe, Ru-Pt, Ru-Pd, etc. [27,28].

In addition, an appropriate support such as SiO_2, Al_2O_3, active carbon, carbon nanotube and zeolite can afford specific interaction with the active Ru sites, and consequently promote the reaction rate, the selectivity as well as the recycling stability [29-32]. Cubic fluorite CeO_2 is frequently employed as the support to stabilize the active metallic sites by providing the strong interaction. The relatively high lattice oxygen mobility and the superior redox ability of CeO_2 support can not

only strongly modify the structural properties of supported metal sites, but also specifically attract with the reaction-relevant intermediates. CeO_2-supported Ru particle has been reported as effective catalysts in hydrogenation reactions such as CO_2-to-CH_4 and amides-to-alcohols [33-35], however, it has not been adopted in the selective hydrogenation of α,β-unsaturated aldehydes and ketones into unsaturated alcohols. Hence, a rational design strategy should be explored to preferentially produce active and durable CeO_2-supported Ru catalysts for the hydrogenation reaction.

In addition to the structural regulation on catalysts, the catalytic hydrogenation performances depend on the reaction conditions, especially the solvent environment. In particularly, the utilization of water as polar solvent has attracted extensive interests in organic synthesis in view of its substantial economic and ecological advantages, as well as separation convenience [36,37]. However, water molecule is in general not an innocent spectator as solvent, and it plays a critical role in the catalytic hydrogenation cycle [38]. It has been recognized that, in contrast to a non-polar solvent, a polar solvent could afford a facile reaction environment to achieve highly selective hydrogenation of C=O groups and production of unsaturated alcohols with similar polarity [39-42]. One of the reasons is identified as the preferential adsorption of hydrophilic C=O bonds over C=C bonds on the catalyst surfaces with the aid of dipolar water solvent [43-45]. The water molecules can coordinate with the homogeneous complex catalysts to form hydroxo species, modifying the structural properties of active metal sites and accelerating hydrogenation or transfer

hydrogenation reactions by hydrophobic effects or hydrogen-bonding interactions with substrates [46-48]. The water molecules can also accelerate the hydrogen diffusion across the surface of metal oxide support, determining the hydrogen spillover process and thus affecting the catalytic hydrogenation activity [49,50]. Furthermore, our previous works have presented an active pathway of water-involved hydrogen exchange, which is coexisted with direct hydrogenation with dissociated H_2 during selective hydrogenation reaction of cinnamaldehyde to cinnamyl alcohol over Pt-based catalysts [51]. The combining results from isotope labeling experiments and theoretical studies have suggested that the water molecule acted as a bridge to facilitate hydrogen exchange between the reactant substrates and the Pt sites with a lower thermodynamic energy barrier. Therefore, water can act as green solvent or catalytic promoter in both homogeneous and heterogeneous hydrogenation reactions, however, great progress in more advantageous use of water remains to be done.

In present work, we finely tune the chemical structure of active Ru sites supported by CeO_2 via the co-modification with tin and boride additives. The Ru/CeO_2-series catalysts with low Ru loadings are applied in the chemoselective hydrogenation reaction of cinnamaldehyde to cinnamyl alchol with pure water as solvent instead of commonly used organic solvents. In addition, a series of detailed characterizations are performed to verify the structural information of Ru-based catalysts. The isotopic experiments of H_2-D_2 and H_2-D_2O exchange as well as D_2O-involved kinetics tests are also carried out for illustrating the catalytic effects of water molecules in the Ru-catalyzed hydrogenation reactions.

2. Experimental

2.1 Materials

Ruthenium chloride hydrate ($RuCl_3 \cdot xH_2O$, 35.0-42.0% in Ru basis), tin chloride dihydrate (98.0-103.0%), boric acid (99.8%), cerium oxide (99.9%), dodecane (98%), ethyl acetate (99.8%), cyclohexane (99.7%), and toluene（99.5%）were purchased from Aladdin Reagent Corp. (Shanghai, China). Cinnamaldehyde (99.0%), phenylpropyl aldehyde (95.0%), cinnamyl alcohol (98.0%), 3-phenylpropanol (99.0%) and isopropanol (99.9%) were obtained from Sigma-Aldrich (Shanghai, China). D_2O (deuteration degree >99.8%) was provided by J&K Scientific (Shanghai, China). H_2 (99.999%), Ar (99.999%) were supplied by Nanjing Special Gas Factory (Nanjing, China). D_2 (99.999%, deuteration degree >99.8%) was obtained from Suzhou Changyou Gas Co., LTD. (Suzhou, China).

2.2. Catalyst preparation

All Ru-based catalysts were prepared by the incipient wetness impregnation method and dry commercial CeO_2 particles were employed as the support. A series of CeO_2-supported Ru, Sn or/and B catalysts with the theoretical molar ratios were synthesized using $RuCl_3$, $SnCl_2$ and H_3BO_3 as the precursors. The ethanol solution containing certain amounts of the precursor salts was incipient impregnated into 1.0 g of the CeO_2 support. After impregnation, the sample was maintained at room temperature for 2 h and then dried overnight in an oven at 100 ^oC. The catalyst was finally obtained after reduction process in a tube furnace under 60 mL of 15 vol.% H_2/Ar flow at 350 ^oC for 3 h with a heating rate of 2 ^oC/min. The accurate loading

amounts of Ru, Sn and B in the catalysts were verified with the ICP-OES analyses and the data were summarized in Table 1. The Ru weight loadings were fixed at approximately 0.7 wt.%, while the molar ratios of Sn and B to Ru were approaching 1:2 for Ru_2Sn_1/CeO_2, Ru_2B_1/CeO_2 and $Ru_2Sn_1B_1/CeO_2$ catalysts.

2.3. Catalyst characterization

Inductively coupled plasma-optical emission spectrometry (ICP-OES, Perkin Elmer, Avio 200) was used to measure the Ru, Sn and B loadings in different catalysts. X-ray diffraction (XRD) patterns were recorded on a Bruker AXS D8 Focus diffractrometer in the 2θ range of 15° to 75° at 40 kV and 40 mA operating conditions. Transmission electron microscope (TEM) images were acquired on a Hitachi HT7700 TEM operated at 120 kV. X-ray photoelectron spectroscopy (XPS) was performed on an Escalab250Xi electron spectrometer (Thermo Scientific) with a monochromatic 150 W Al K_α radiation source. The Brunauer-Emmett-Teller (BET) specific surface areas were obtained from the N_2 adsorption-desorption measurements performed at -196 ^oC on a Quantachrome Autosorb-iQ3 adsorption analyzer. The samples were first degassed under vacuum at 200 ^oC for 8 h. The Raman spectra were recorded on a Horiba HR Evolution spectrometer with 532 nm excitation laser source.

Temperature programmed reduction (TPR) was performed on a chemical adsorption analyzer (AutoChem 2920, Micromeritics) with a U-shaped quartz tube. 80 mg of catalyst was loaded and then pretreated in 30 mL/min of Ar flow for 1.5 h at 300 ^oC. After cooling down to room temperature and reaching a steady state, the reduction TCD signal was started to record with heating sample to 550 ^oC in 20

mL/min 10 vol.% H_2/Ar at a specific rate of 10 ^oC.

The diffuse reflectance infrared fourier transform spectroscopy (DRIFTs) of CO adsorption was performed on a Nicolet iS10 FTIR spectrometer equipped with a Harrick diffuse reflection cell and a liquid nitrogen-cooled MCT/A detector. The sample was pretreated at 300 ^oC for 90 min and cooled down to 25 ^oC in 30 mL/min of Ar flow before CO adsorption experiment. The background spectrum was collected after 60 min in 30 mL/min of Ar gas, followed by introducing 10 mL/min of CO flow to start the chemisorption. After the CO adsorption lasting for 30 min, the sample was further purged with 30 mL/min of Ar flow for 30 min and then the spectrum was acquired. Accumulating 16 scans and a spectral resolution of 4 cm^{-1} were set for all recorded spectra.

2.4. Catalytic hydrogenation reaction

The cinnamaldehyde hydrogenation reaction was proceeded in a 50 mL Hastelloy batch reactor (NS-50-C276, Anhui Kemi Machinery Technology Co., Ltd.) with a Teflon liner. Catalyst (20 mg), and CALD (200 μL) in solvent (10 mL) were added into the reactor. The residual air inside the reactor was removed by repeatedly pressurizing and releasing H_2 gas. The reaction was performed at 60 or 100 ^oC under 1 or 20 bar of H_2. For eliminating the external mass transfer limitation, 700 rpm of stirring speed was used in all the reactions. After the reaction was completed, the reactor was cooled to room temperature and the high-pressure H_2 was released. The catalyst powder was separated by 1400 rpm centrifugation. All the liquid products were analyzed using a flame ionization detector (FID)-equipped gas chromatograph

(GC, Agilent, 7890B). A CP-WAX 52 CB column (30 m × 0.25 mm × 0.25 μm) was armed in the GC for products separation. The byproducts were identified by a gas chromatography-mass spectrometry (GC-MS, Agilent, 6890N-5973). Tetradecane was served as the internal standard and the carbon balance was kept >99% in all the hydrogenation reactions. For recycling tests, the reused catalyst was hot filtrated and washed with ethanol several times after each reaction run, and then kept drying before next reaction run. The catalytic reaction data were calculated based on the the following formulas:

$$\text{Conversion} = [\ N_{in}(\text{CALD}) - N_{out}(\text{CALD})\ ] / N_{in}(\text{CALD}) \times 100\%$$

$$\text{Selectivity}(i) = N_{out}(i) / \Sigma_i N_{out}(i) \times 100\%$$

$$\text{Carbon balance} = [\ N_{out}(\text{CALD}) + \Sigma_i N_{out}(i)\ ] / N_{in}(\text{CALD}) \times 100\%$$

$$\text{Specific reaction rate} = [\ \text{Conversion} \times N_{in}(\text{CALD})\ ] / [\ \text{Time} \times N_{total}(\text{Ru})\ ]$$

Where i represented hydrogenation products; $N_{out}(i)$ was the molar amount of corresponding product i; $N_{total}(\text{Ru})$ was the molar number of total Ru atoms in employed catalyst.

The experimental CALD concentration as a function of time were plotted according to a rate law of first order with respect to CALD. The reaction rate constant *k* was calculated by the linear fitting method with the following formula:

$$\ln (C_t / C_0) = - k \times t$$

where C_t represented the CALD concentration at reaction time t, and C_0 was the initial CALD concentration.

2.5. Isotope labeling measurement

H_2-D_2 exchange experiments were performed in a fixed-bed reactor with a quartz tube (8 mm in inner diameter). A 10 mg portion of catalyst was loaded in the reactor and the feeding gases consisted of 8 mL/min of H_2, 8 mL/min of D_2 and 36 mL/ min of Ar balance gas. Prior to the exchange reaction, the sample was pretreated in Ar flow at 120 ^oC for 30 min. After cooling to 40 ^oC, the gas flow was switched to H_2-D_2-Ar mixture to start the H_2-D_2 exchange reaction. The exchange reaction-relevant gases of H_2, HD and D_2 were analyzed with a mass spectrometer (MS, QGA, Hiden Analytical Ltd.).

H_2-D_2O exchange measurements were performed in a batch reactor operated at 100 ^oC and 20 bar of H_2. The loading amount of Ru-based catalyst was 20 mg and the exchange reaction was lasted for 2 h. After the reaction was completed and the reactor was cooled down, the gaseous mixture inside the reactor, including H_2, D_2 and HD, was collected with a gas bag and then was analyzed on the MS.

Isotope-labeling kinetic studies were also performed in a batch reactor. The reaction conditions were similar to the regular catalytic hydrogenation reaction tests except of using D_2O to replace H_2O as solvent. The certain conditions were 20 mg of Ru-based catalyst, 200 μL of CALD, 10 mL of D_2O solvent, 60 or 100 ^oC, 1 or 20 bar of H_2, and 2 h of time duration. The liquid products containing deuterated molecules were analyzed on the GC-MS. The reference experiments were also carried out to clarify the exchange degrees between three kinds of primary hydrogenated products (CALA, HCALD and HCALA) and pure D_2O in the absence of the Ru catalysts. The reference experiment of exchange between D_2 and products was further performed in

the presence of catalyst (conditions: 20 mg of $Ru_2Sn_2B_1/CeO_2$ catalyst, 60 μL of product, 10 mL of n-dodecane, 100 °C, 1 bar of D_2, and 12 h of time duration).

3. Results and discussion

3.1. Catalytic performance of Ru catalysts in water

These CeO_2-supported Ru catalysts with various compositions were applied in the selective hydrogenation of cinnamaldehyde (CALD) to cinnamyl alcohol (CALA) at a relatively low temperature (60 °C) with pure water as the solvent. For evaluating the specific reaction rate under a comparable level, the CALD conversion in each test was kept at approximately 40% through reregulating the reaction time duration and/or catalyst amount. As presented in **Fig. 1A**, monometallic Ru/CeO_2 catalyst displayed an unsatisfactory hydrogenation selectivity towards CALA at 60.2% and a lower specific reaction rate of 11.0 h^{-1} (consumed CALD moles derived by total Ru mole in the catalyst per hour). The modification with B additive in Ru_2B_1/CeO_2 catalyst led to a decreased CALA selectivity at 47.7%, however, it caused near two times improvement in the reaction rate to 29.3 h^{-1}, as compared to Ru/CeO_2 catalyst. For Sn-modified bimetallic Ru_2Sn_1/CeO_2 catalyst, both the reaction rate and CALA selectivity further increased up to 118.2 h^{-1} and 71.8%, respectively. In contrast to monometallic and binary Ru-based catalysts, ternary $Ru_2Sn_1B_1/CeO_2$ catalyst exhibited a significantly promoted catalytic hydrogenation performance that its specific reaction rate and the CALA selectivity could reach up to 223.2 h^{-1} and 89.7%, respectively.

The CALD hydrogenation reaction was performed in the kinetic region to further

compare the catalytic properties of Ru_2Sn_1/CeO_2 and $Ru_2Sn_1B_1/CeO_2$ catalysts. The reaction rate constants (*k*) over these two catalysts were measured in the initial reaction stages, and the linear dependence of $\ln(C_t/C_0)$ as a function of reaction time suggested that the catalytic reaction followed psudo first-order with respect to CALD reactant, as shown in **Fig. 1B**. The $Ru_2Sn_1B_1/CeO_2$ catalyst displayed a *k* value of 0.289 h^{-1}, which was two times as high as that of Ru_2Sn_1/CeO_2 catalyst (k=0.133 h^{-1}). In addition, the CALA selectivity of Ru_2Sn_1/CeO_2 catalyst was always less than 80% during the whole reaction stages, whereas $Ru_2Sn_1B_1/CeO_2$ catalyst can maintain a superior CALA selectivity beyond 90% in the hydrogenation reaction. These results indicated that the CeO_2-supported Ru catalyst jointly decorated with Sn and B species could efficiently catalyze the selective hydrogenation reaction of CALD to CALA in water solvent.

The solvent effect cannot be ignored in the heterogeneous catalysis, especially in the catalytic hydrogenation of α,β-unsaturated aldehydes and ketones to α,β-unsaturated alcohols [42,51]. The optimized $Ru_2Sn_1B_1/CeO_2$ catalyst was employed to verify the superior catalytic properties in pure water over varieties of organic solvents in CALD hydrogenation reactions. With same reaction conditions and time durations, poor CALA selectivity at less than 50% and low CALD conversion at less than 30% were obtained in those common organic solvents such as ethyl acetate, cyclohexane, n-dodecane and toluene, as shown in **Fig. 2A**. Specifically, isopropanol has been served as the most frequently used solvent in the hydrogenation reaction of unsaturated aldehydes, nonetheless, the CALA selectivity and the CALD conversion

of $Ru_2Sn_1B_1/CeO_2$ catalyst with isopropanol as solvent were only 75.0% and 24.0%, respectively, which were still dramatically inferior to that with water as the solvent (93.9% for CALA selectivity and 96.0% for CALD conversion). When small amount of water was added into isopropanol (molar ratio of water to isopropanol=5:100, 10:100), obvious increase of conversion (29.5% and 33.0%) was observed, suggesting the acceleration effect of water molecules in the hydrogenation reactions. The first order reaction rate constants (*k*) in water and isopropanol solvents were further measured in the kinetic reaction regions. The *k* value of 0.289 h^{-1} was observed in water, which was over five times higher than that of 0.051 h^{-1} obtained in isopropanol solvent, as shown in **Fig. 2B**. These results clearly demonstrated that water solvent molecules played a critical role in enhancing both catalytic activity and hydrogenation selectivity in CALD hydrogenation reaction. The catalytic effects of water would be worth more detailed discusses in the following sections.

The catalytic stability and reusability of the optimal ternary $Ru_2Sn_1B_1/CeO_2$ catalyst was also investigated by repeated reaction tests in water solvent, and the performances were presented in **Fig. 3**. After each recycling reaction run, the catalyst was hot filtrated and washed with ethanol several times, and then kept drying overnight till the next cycle run. Both the CALD conversion and the CALA selectivity were maintained approaching 90% in six-cycle runs, suggesting great catalytic and structural stabilities of the $Ru_2Sn_1B_1/CeO_2$ catalyst in aqueous phase selective hydrogenation of CALD to CALA.

3.2 Structure characterization of CeO_2-supported Ru catalysts

A series of CeO_2-supported Ru catalysts were prepared by the incipient wetness impregnation method. The dry commercial CeO_2 nanoparticles (NPs) were employed as the support and the Ru loadings were fixed at approximately 0.7 wt.% for all the Ru-based catalysts, which were confirmed by the ICP-OES analyses results as listed in Table 1. The molar ratios of Ru:Sn and Ru:Sn:B were approaching 2:1 and 2:1:1 for Ru_2Sn_1/CeO_2 and $Ru_2Sn_1B_1/CeO_2$ catalysts, respectively (**Table 1**). Since these Ru catalysts exhibited distinctly different catalytic performances in the CALD hydrogenation reactions, their composition and structure were carefully characterized to gain a clear physical chemical insight on the relevance between the catalytic activity and the catalyst structure, namely the nature in structure-function relations.

The powder XRD patterns in **Fig. 4A** revealed that only the standard diffraction peaks of the cubic fluorite CeO_2 phase were observed on either pure CeO_2 support or the Ru-based catalyst. The legible peaks at 28.4º, 32.9º, 47.3º, 56.2º and 58.9º were corresponding to the (111), (200), (220), (311), and (222) planes of CeO_2, respectively. Neither metallic Ru nor RuO_2 phase was observed in these supported Ru catalysts. In addition, the diffraction peaks of SnO_2, Sn or B-related phases were not found in the XRD patterns of Sn or B-containing catalysts, possibly due to the relatively low loading amounts or high dispersion of Ru, Sn and B species on CeO_2 surfaces. The nitrogen adsorption isotherms exhibited similar specific BET surface areas for the catalysts (approximately 20 m^2/g, **Table 1**), suggesting that the impregnated deposition of Ru, Sn or B species cannot apparently vary the surface area of CeO_2 NP supports. The visible (532 nm) Raman spectra of the CeO_2-supported

catalysts in **Fig. 4B-C** were dominated by a strong peak at 461 cm^{-1} with a weak band at 1172 cm^{-1}, which were corresponding to the F_{2g} symmetry vibrational mode and the second-order longitudinal optical (2LO) mode of the fluorite CeO_2 lattice, respectively [52]. Neither defect-induced band at ca. 590 cm^{-1} nor bands of surface oxygen species at 830, 890 or 1139 cm^{-1} was observed on these catalysts, indicating that there was no abundant oxygen-vacancies and adsorbed oxygen species on the catalyst surfaces [53,54]. In addition, the typical peaks of A_{1g} and B_{2g} vibration modes of Sn-O bonds in crystalline SnO_2 (at ca. 632 and 724 cm^{-1}, respectively) were absent on the Raman spectra, suggesting the absence of bulk SnO_2 species in Sn-containing catalysts [54-56]. The TEM images in **Fig. 5** illustrated that the Ru nanoparticles could highly disperse on the CeO_2 support in all Ru-based catalysts. For CeO_2-supported monometallic Ru NPs, the average particle size was comparatively small, 2.3±0.7 nm as shown in **Fig. 5A-B**. The modification of Sn or B additives could not cause obvious changes in the particle size distributions. As shown in **Fig. 5C-F**, the similar particle sizes were observed at 2.1±0.7 and 2.6±0.8 nm for Ru_2Sn_1/CeO_2 and $Ru_2Sn_1B_1/CeO_2$ catalyst, respectively.

XPS measurements in **Fig. 6** presented the electronic states of Ru and Sn species on the Ru-based catalysts surfaces. Since the signal of Ru 3d 3/2 orbit overlapped with that of C 1s orbit, the Ru 3d 5/2 peak was used to determine the chemical states of Ru species in all the catalysts. The metallic Ru^0 and oxidative $Ru^{\delta+}$ surface species were confirmed to be coexisted in monometallic Ru/CeO_2 catalyst, which both metallic Ru^0 peak at 280.1 eV in binding energy (BE) and oxidative $Ru^{\delta+}$ peak at

281.6 eV were presented in the spectrum in **Fig. 6A** [57,58]. The peak corresponding to Ru^0 surface species disappeared on bimetallic Ru_2Sn_1/CeO_2 catalyst, however, the peak of $Ru^{\delta+}$ species was distinguishable in the XPS spectrum (**Fig. 6B**). In the case of the ternary $Ru_2Sn_1B_1/CeO_2$ catalyst, two peaks of Ru^0 and $Ru^{\delta+}$ species appeared in parallel, as shown in **Fig. 6C**. The calculated atomic ratios of $Ru^0/Ru^{\delta+}$ in the Ru-based catalysts were summarized in **Table 1**, which the values were 80/20, 0/100 and 26/74, for Ru/CeO_2, Ru_2Sn_1/CeO_2 and $Ru_2Sn_1B_1/CeO_2$ catalyst, respectively. XPS results also provided the distributions of surface Sn-related species, and the coexisted metallic Sn^0 and oxidative SnO_x species were observed on all Sn-containing catalysts, as presented in **Fig. 6D-F**. Furthermore, SnO_x species dominated over metallic Sn^0, which the ratios of $Sn^0/Sn^{2+/4+}$ were 10/90 and 24/76, for Ru_2Sn_1/CeO_2 and $Ru_2Sn_1B_1/CeO_2$ catalyst, respectively **(Table 1)**. According to the XPS analyses results, the addition of SnO_x species led to the disappearance of metallic Ru^0 surface species in Ru_2Sn_1/CeO_2 catalyst, might due to full coverage of SnO_x on Ru atoms or incorporation of Ru into SnO_x matrix. The further modification with B species in $Ru_2Sn_1B_1/CeO_2$ catalyst allowed the partial exposure of metallic Ru^0 and Sn^0 sites on the surface, possibly attributed to the electric neutrality demanding in the presence of positive B^{3+} species [57,59].

To investigate the structural redox properties of various phases on the catalyst surface and their interactions, H_2-TPR analyses were performed on these series of Ru catalysts. As presented in **Fig. 7**, only one prominent peak at ca. 460 ^oC was observed on pure CeO_2 support, which was assigned to the reduction of surface oxygen species

on CeO_2 [60]. A wide hydrogen-absorption reduction region at 180-450 ^oC with a peak at 250 ^oC was attributed to the reduction of SnO_x species with strong interactions with the CeO_2 support for the Sn/CeO_2 (Sn: 0.4 wt.%) catalyst. A peak of CeO_2-stabilized RuO_x species at 65 ^oC was observed on the monometallic Ru/CeO_2 catalyst. Modification of Sn additive on Ru in the Ru_2Sn_1/CeO_2 catalyst exhibited two overlapping peaks at 100 and 160 ^oC, located in the middle of each reduction peaks of RuO_x and SnO_x surface species. The enhanced anti-reduction ability reflected the formation of SnO_x matrix-immobilized RuO_x structure with strong interactions between these two components. $Ru_2Sn_1B_1/CeO_2$ catalyst with further B modifications revealed a similar H_2-TPR pattern except of a slightly shifted reduction peak at 100 ^oC. In addition, the individual reduction behavior of RuO_x species was evidently distinguishable, compared to that in Ru_2Sn_1/CeO_2 catalyst, suggesting that the B additives could effectively introduce migration of Ru atoms inside SnO_x matrix into the surface. This result was also conformed to the varying tendency of $Ru^0/Ru^{\delta+}$ ratio from XPS spectral results.

The DRIFT spectra of the chemisorption of CO probe molecules provided sensitive structural information of the Ru sites on the catalyst surface as well as the synergistic effect of RuSnB ternary species. The experiments were carried out at 25 ^oC and the in-situ DRIFT spectra were recorded after CO desorption in the Ar flow. The spectra in **Fig. 8** were displayed in Kubelka-Munk (K-M) unit and fitted with five types of the chemisorption configurations of CO on Ru sites, as summarized in **Table 2**. Two distinct peaks at relatively higher frequencies (HF) of 2140 and 2088 cm^{-1} and

three peaks at lower frequencies (LF) of 2055, 2017 and 1969 cm^{-1} could be precisely fitted with three Ru catalysts. The LF peak at 1969 cm^{-1} was assigned to the bridge-bonded CO on the metallic Ru^0 atoms, and the LF peaks at 2017 and 2055 cm^{-1} were associated with the adsorption of dicarbonyl CO species on oxidative Ru^{2+} site and on the metallic Ru^0 site, respectively [61-63]. Two HF peaks at 2088 and 2140 cm^{-1} were corresponding to the adsorption models of CO species on the oxidative $Ru^{\delta+}$ sites, including dicarbonyl, tricarbonyl and linear models [61-63].

The CO-adsorption DRIFT spectral features clearly indicated different distributions of metallic Ru^0 and oxidative $Ru^{\delta+}$ surface sites in these three Ru-based catalysts. The ratios of $Ru^{\delta+}/Ru^0$ in Ru/CeO_2, Ru_2Sn_1/CeO_2 and $Ru_2Sn_1B_1/CeO_2$ catalysts were 12.3/87.7, 84.9/15.1 and 84.6/15.4, respectively, according to the fitted peak areas. Dramatically reduced amount of metallic Ru^0 surface sites in Ru_2Sn_1/CeO_2 and $Ru_2Sn_1B_1/CeO_2$ catalysts compared to that in Ru/CeO_2 catalyst was in accord with the H_2-TPR results that part of Ru atoms were incorporated into the SnO_x matrix. It also agreed with the H_2-TPR results that B-modified $Ru_2Sn_1B_1/CeO_2$ catalyst had a slightly increased proportion of metallic Ru^0 surface sites than Ru_2Sn_1/CeO_2 catalyst. Furthermore, the role of B additive in the electronic modification of Ru was evidenced by the blue-shift of the CO-adsorption characteristic peaks [64, 65]. For instance, either bridge-bonded CO-Ru^0 peak or dicarbonyl CO-Ru^{2+} peak shifted towards higher frequencies over $Ru_2Sn_1B_1/CeO_2$ catalyst in contrast with Ru_2Sn_1/CeO_2 catalyst (1969 to 1971 cm^{-1} and 2017 to 2022 cm^{-1}, respectively). Therefore, these combined characterization results presented that

the optimal $Ru_2Sn_1B_1/CeO_2$ catalyst might consist of RuSn alloy phase encapsulated by SnO_x-matrix on CeO_2 support. The Sn additives largely modify the surface electron density of active Ru sites for improving the adsorption and reactivity of the C=O bond, while the geometric effect of intermetallic RuSn-encapsulated SnO_x species can play a part in the suppression of C=C bond adsorptive hydrogenation [66-68]. The electronic and catalytic properties of Ru could be further modified by their interaction with Sn and B promoters for most promising hydrogenation catalysts based on ternary RuSnB compositions [57-59, 64, 69].

3.3. Ru site-determined H_2 dissociation

Detailed kinetic studies have presented that the reaction rates of metal-catalyzed direct hydrogenation of α,β-unsaturated aldehydes obeyed the Langmuir-Hinshelwood kinetic law [70]. Consequently, the dissociative activation ability of H_2 molecules adsorbed on the Ru catalyst surface should be one of the most critical factor to consider. The H_2-D_2 exchange reaction rates over three Ru-based catalysts were measured at 25 ^oC with an online MS. As shown in **Fig. 9**, the exchange product HD could be steadily produced with the co-feeding of 1:1 (in vol.%) H_2 and D_2, however, significantly different rates of HD generation were observed on three Ru catalysts. Specifically, the HD generation rate of the monometallic Ru/CeO_2 catalyst was 13.5 and 4.4 times as high as that of Ru_2Sn_1/CeO_2 and $Ru_2Sn_1B_1/CeO_2$ catalysts, respectively, possessing the superior ability of H_2 dissociation. The weaker H_2 dissociation ability of Sn-modified Ru_2Sn_1/CeO_2 catalyst might be ascribed to reduced metallic Ru sites exposed on the catalyst surface. This result was associated

with the coverage of surface Ru atoms by the SnO_x species, which was also in agreement with the CO-adsorption DRIFT spectrum and H_2-TPR pattern. Furthermore, the modification of B additive in $Ru_2Sn_1B_1/CeO_2$ catalyst led to higher exposure degree of Ru atoms and thus higher H_2 dissociation rate compared to Ru_2Sn_1/CeO_2 catalyst.

On the other hand, the monometallic Ru/CeO_2 catalyst showed the greatest H_2 dissociation ability among three Ru-based catalysts, nonetheless, it showed the lowest CALD conversion in the high-pressure hydrogenation reaction, indicating that H_2 dissociative activation should not be the rate-limiting step in Ru-catalyzed CALD hydrogenation reaction. This result was also verified by the fact that the hydrogenation activity was still in the consequence of Ru/CeO_2 (15.0 h^{-1}) < Ru_2Sn_1/CeO_2 (37.6 h^{-1}) < $Ru_2Sn_1B_1/CeO_2$ (43.3 h^{-1}), when ambient pressure (1 bar) of H_2 was adopted in the hydrogenation reactions. These observations were in line with the previous report that the hydrogenation reactions of unsaturated aldehydes and ketones ordinarily followed a near first-order reaction kinetics with respect to H_2, involving the dissociated H species weakly bonding on the metal surface [71-73].

3.4. H_2O-involved hydrogenation

As described in above section, the utilization of water as solvent could facilitate selective hydrogenation of CALD to CALA over Ru-based catalysts. In addition to afford a polar reaction environment, water has also been demonstrated to induce a water-mediated hydrogen-exchange reaction route for accelerating the CALD hydrogenation reaction on alloyed PtFe catalysts, which was coexisted with direct H_2

dissociative hydrogenation route [51]. It could be expected that water-involved reaction pathway occurred in the Ru-catalyzed hydrogenation of CALD. Therefore, pure deuterium oxide (D_2O) was employed instead of H_2O to further study the catalytic role of water in the reactions.

The control experiments of exchange between the relevant reactants and D_2O were first carried out in the absence of the Ru catalysts. No MS signals of the deuterated molecules through H-D exchange were emerged for CALA, HCALD and HCALA, suggesting that alkenyl and aldehyde as well as hydroxyl groups could not interact with D_2O molecules. The intensity ratio of the peak at m/z=M+1 (M=molecular weight) to the molecular ion peak at m/z=M were extremely low (<0.2) for all three hydrogenation products in the reference tests, as shown in **Fig. 10A-C**. The control experiments of exchange between the main products and D_2 gas were further performed in the presence of $Ru_2Sn_1B_1/CeO_2$ catalyst. The MS spectra displayed that the peak intensity ratio of m/z=M+1 to m/z=M did not obviously increase as compared to that of pristine molecules, suggesting that almost no product molecule has exchanged with D species dissociated from D_2 on the $Ru_2Sn_1B_1/CeO_2$ catalyst surfaces. However, the peak intensity ratio of m/z 135:134 for the primary product CALA was remarkably increased up to 1.1 after $Ru_2Sn_1B_1/CeO_2$-catalyzed hydrogenation reaction at 100 ^oC in D_2O solvent, as shown in **Fig. 10D**, suggesting that a large number of the deuterated CALA molecules has produced during the reaction. This result demonstrated that the D atom in the deuterated CALA product could derive from the D_2O-involved hydrogenation reaction process rather than a

simple H-D exchange process between D_2O and formed CALA molecules. In addition, the deuteration of both HCALD and HCALA that served as the C=C hydrogenated product and the full hydrogenated product, respectively, was also observed after the reaction. The peak intensity ratio of m/z 135:134 for HCALD and the ratio of m/z 137/136 for HCALA reached to 1.7 and 2.4, respectively, as presented in **Fig. 10E-F**, greatly higher than the values (0.1-0.2) obtained in reference tests. These observations proved that D_2O was involved not only in the C=O hydrogenation, but also in the C=C hydrogenation during $Ru_2Sn_1B_1/CeO_2$-catalyzed reaction. Furthermore, such D_2O-mediated reaction pathway could occur even under varied reaction temperature and H_2 pressure. For CALA, HCALD and HCALA products in the hydrogenation reaction at 60 ^oC under 1 bar of H_2, their peak intensity ratios of m/z (M+1)/M were 0.9, 1.2 and 0.9, respectively, which were still obviously larger than the ratios observed in the reference tests.

Fig. 11 presented the signals of deuterated molecules in the MS spectra for all of three kinds of products (CALA, HCALD and HCALA) in the CALD hydrogenation reactions catalyzed by monometallic Ru/CeO_2 and bimetallic Ru_2Sn_1/CeO_2 catalysts, evidencing that the D_2O-involved D-exchange could serve as a crucial pathway that coexisted with the direct H_2 dissociative hydrogenation pathway in the Ru-catalyzed reactions (Scheme 2). Either of these two pathways could definitely influence the whole hydrogenation reaction, and it is reasonable to expect that the H_2O-involved H-exchange (as well as D-exchange for D_2O) process should be determined by the Ru sites.

To prove this view, H_2-D_2O exchange experiments were performed on three types of CeO_2-supported Ru catalysts. The yields of gaseous HD and D_2 products during the exchange reactions were displayed in **Fig. 12**. The $Ru_2Sn_1B_1/CeO_2$ catalyst showed higher generation rates of HD and D_2 than monometallic Ru/CeO_2 catalyst, while the bimetallic Ru_2Sn_1/CeO_2 catalyst showed the lowest rates among three Ru catalysts. The relatively poor H_2-dissociation ability of Ru_2Sn_1/CeO_2 catalyst, which was clarified by previously discussed H_2-D_2 exchange results, possibly caused the lowest H_2-D_2O exchange reaction rate. On the other hand, in view of that the efficiency of the H_2 dissociative activation of $Ru_2Sn_1B_1/CeO_2$ catalyst has been demonstrated lower than that of Ru/CeO_2 catalyst, reflecting that $Ru_2Sn_1B_1/CeO_2$ catalyst was more capable of efficiently achieving water dissociative activation compared to Ru/CeO_2 catalyst. Therefore, $Ru_2Sn_1B_1/CeO_2$ catalyst could maximum the formation rates of these deuterated hydrogenation products as compared with Ru/CeO_2 and Ru_2Sn_1/CeO_2 catalysts, under similar deuteration degrees of the primary products in the D_2O-involved hydrogenation reactions.

4. Conclusions

In summary, the co-modification of Sn and B additives on CeO_2-supported Ru sites by geometric and electronic effects can afford significantly enhanced catalytic properties with respect to both activity (the specific reaction rate reaches 223 h^{-1}) and selectivity (90%) in aqueous phase hydrogenation reaction of CALD to CALA. The detailed characterization results reveal that the ternary $Ru_2Sn_1B_1/CeO_2$ catalyst is composed of SnO_x-encapsulated RuSn alloy on CeO_2 surface. The isotopic labeling

kinetic experiments demonstrate that water-mediated hydrogen-exchange route is coexisted with direct hydrogenation route with dissociated H_2 during Ru-catalyzed hydrogenation reactions. The performances in H_2-D_2 and H_2-D_2O exchange reactions suggest that the activation of H_2 molecules is not the rate-limiting step, nonetheless, the activation of water molecules can determine the water-involved hydrogenation process. This work shows a promising strategy of synergetic effect between structural modification and water assistance for metal-catalyzed hydrogenation reactions of α,β-unsaturated aldehydes and ketones into unsaturated alcohols.

Acknowledgements

NJTech group appreciates the financial support from the National Natural Science Foundation of China (21802070, and the support from the Jiangsu Provincial Department of Education and Natural Science Foundation (17KJB150021 and BK20170986). IMR group thanks the National Natural Science Foundation of China (91645114, 21573256, 21761132010) for the financial support. We are grateful for the support from Nanjing Technology Innovation Fund for Overseas Talents.

References

[1] P. Gallezot, D. Richard, Selective hydrogenation of α,β-unsaturated aldehydes, Catal. Rev. 40 (1998) 81-126.

[2] Y. Yuan, Y. Siyu, W. Mengnan, L. Shujie, Y. Ning, Recent progress in chemoselective hydrogenation of alpha,beta-unsaturated aldehyde to unsaturated

alcohol over nanomaterials, Curr. Org. Chem. 17 (2013) 400-413.

[3] P. Claus, Selective hydrogenation of α,β-unsaturated aldehydes and other C=O and C=C bonds containing compounds, Top. Catal. 5 (1998) 51-62.

[4] P. Mäki-Arvela, J. Hájek, T. Salmi, D.Y. Murzin, Chemoselective hydrogenation of carbonyl compounds over heterogeneous catalysts, Appl. Catal. A-Gen. 292 (2005) 1-49.

[5] J.W. Medlin, Understanding and controlling reactivity of unsaturated oxygenates and polyols on metal catalysts, ACS Catal. 1 (2011) 1284-1297.

[6] M.S. Ide, B. Hao, M. Neurock, R.J. Davis, Mechanistic insights on the hydrogenation of α,β-unsaturated ketones and aldehydes to unsaturated alcohols over metal catalysts, ACS Catal. 2 (2012) 671-683.

[7] B. Wu, H. Huang, J. Yang, N. Zheng, G. Fu, Selective hydrogenation of alpha,beta-unsaturated aldehydes catalyzed by amine-capped platinum-cobalt nanocrystals, Angew. Chem. Int. Ed. 51 (2012) 3440-3443.

[8] G. Kennedy, L.R. Baker, G.A. Somorjai, Selective amplification of C=O bond hydrogenation on Pt/TiO_2: catalytic reaction and sum-frequency generation vibrational spectroscopy studies of crotonaldehyde hydrogenation, Angew. Chem. Int. Ed. 53 (2014) 3405-3408.

[9] M. Zhao, K. Yuan, Y. Wang, G. Li, J. Guo, L. Gu, W. Hu, H. Zhao, Z. Tang, Metal-organic frameworks as selectivity regulators for hydrogenation reactions, Nature 539 (2016) 76-80.

[10] Y. Zhu, H. Qian, B. A. Drake, R. Jin, Atomically Precise $Au_{25}(SR)_{18}$ nanoparticles as catalysts for the selective hydrogenation of α,β-unsaturated ketones and aldehydes, Angew. Chem. Int. Ed. 49 (2010) 1295-1298.

[11] Y. Dai, Y. Wang, B. Liu, Y. Yang, Metallic nanocatalysis: an accelerating

seamless integration with nanotechnology, Small 11 (2015) 268-289.

[12] H. Lin, J. Zheng, X. Zheng, Z. Gu, Y. Yuan, Y. Yang, Improved chemoselective hydrogenation of crotonaldehyde over bimetallic AuAg/SBA-15 catalyst, J. Catal. 330 (2015) 135-144.

[13] K.H. Dostert, C.P. O'Brien, F. Ivars-Barcelo, S. Schauermann, H.J. Freund, Spectators control selectivity in surface chemistry: acrolein partial hydrogenation over Pd, J. Am. Chem. Soc. 137 (2015) 13496-13502.

[14] Q. Hu, S. Wang, Z. Gao, Y. Li, Q. Zhang, Q. Xiang, Y. Qin, The precise decoration of Pt nanoparticles with Fe oxide by atomic layer deposition for the selective hydrogenation of cinnamaldehyde, Appl. Catal. B-Environ. 218 (2017) 591-599.

[15] M. Lashdaf, A.O.I. Krause, M. Lindblad, M. Tiitta, T. Venäläinen, Behaviour of palladium and ruthenium catalysts on alumina and silica prepared by gas and liquid phase deposition in cinnamaldehyde hydrogenation, Appl. Catal. A-Gen. 241 (2003) 65-75.

[16] W.O. Oduro, N. Cailuo, K.M.K. Yu, H. Yang, S.C. Tsang, Geometric and electronic effects on hydrogenation of cinnamaldehyde over unsupported Pt-based nanocrystals, Phys. Chem. Chem. Phys. 13 (2011) 2590-2602.

[17] J. Shi, M. Zhang, W. Du, W. Ning, Z. Hou, SnO_2-isolated Pt_3Sn alloy on reduced graphene oxide: an efficient catalyst for selective hydrogenation of C=O in unsaturated aldehydes, Catal. Sci. Technol. 5 (2015) 3108-3112.

[18] Z. Guo, C. Xiao, R.V. Maligal-Ganesh, L. Zhou, T.W. Goh, X. Li, D. Tesfagaber, A. Thiel, W. Huang, Pt Nanoclusters confined within metal-organic framework cavities for chemoselective cinnamaldehyde hydrogenation, ACS Catal. 4 (2014) 1340-1348.

[19] F. Ammari, An emergent catalytic material: Pt/ZnO catalyst for selective hydrogenation of crotonaldehyde, J. Catal. 221 (2004) 32-42.

[20] S. Bhogeswararao, D. Srinivas, Intramolecular selective hydrogenation of cinnamaldehyde over CeO_2-ZrO_2-supported Pt catalysts, J. Catal. 285 (2012) 31-40.

[21] E. Gebauerhenke, J. Grams, E. Szubiakiewicz, J. Farbotko, R. Touroude, J. Rynkowski, Pt/Ga_2O_3 catalysts of selective hydrogenation of crotonaldehyde, J. Catal. 250 (2007) 195-208.

[22] X. Hong, B. Li, Y. Wang, J. Lu, G. Hu, M. Luo, Stable Ir/SiO_2 catalyst for selective hydrogenation of crotonaldehyde, Appl. Surf. Sci. 270 (2013) 388-394.

[23] A.J. Plomp, H. Vuori, A.O.I. Krause, K.P. de Jong, J.H. Bitter, Particle size effects for carbon nanofiber supported platinum and ruthenium catalysts for the selective hydrogenation of cinnamaldehyde, Appl. Catal. A-Gen. 351 (2008) 9-15.

[24] G.C.S. Galvagno, G. Neri, A. Donato, R. Pietropaolo, Hydrogenation of cinnamaldehyde over Ru/C catalysts: effect of Ru particle size, J. Mol. Catal. 64 (1991) 237-246.

[25] G. Neri, L. Mercadante, C. Milone, R. Pietropaolo, S. Galvagno, Hydrogenation of citral and cinamaldehyde over bimetallic Ru-Me/Al_2O_3 catalysts, J. Mol. Catal. A-Chem. 108 (1996) 41-50.

[26] T.-N. Ye, J. Li, M. Kitano, M. Sasase, H. Hosono, Electronic interactions between a stable electride and a nano-alloy control the chemoselective reduction reaction, Chem. Sci. 7 (2016) 5969-5975.

[27] J. Teddy, A. Falqui, A. Corrias, D. Carta, P. Lecante, I. Gerber, P. Serp, Influence of particles alloying on the performances of Pt-Ru/CNT catalysts for selective hydrogenation, J. Catal. 278 (2011) 59-70.

[28] J. Qiu, X.Wang, H. Han, C. Liang, C. Li, Selective hydrogenation of

cinnamaldehyde over carbon nanotube supported Pd-Ru catalyst, React. Kinet. Catal. Lett. 88 (2006) 269-275.

[29] A. Jung, A. Jess, T. Schubert, W. Schütz, Performance of carbon nanomaterial (nanotubes and nanofibres) supported platinum and palladium catalysts for the hydrogenation of cinnamaldehyde and of 1-octyne, Appl. Catal. A-Gen. 362 (2009) 95-105.

[30] H. Shen, H. Tang, H. Yan, W. Han, Y. Li, J. Ni, Geometric effect of Ru/HSAG@mSiO$_2$: a catalyst for selective hydrogenation of cinnamaldehyde, RSC Adv. 4 (2014) 30180-30185.

[31] N. Mager, P. Libioulle, S. Carlier, S. Hermans, Water-soluble single source precursors for homo- and hetero-metallic nanoparticle catalysts supported on nanocarbons, Catal. Today 301 (2018) 153-163.

[32] Y. Yan, Q. Wang, C. Jiang, Y. Yao, D. Lu, J. Zheng, Y. Dai, H. Wang, Y. Yang, Ru/Al$_2$O$_3$ catalyzed CO$_2$ hydrogenation: oxygen-exchange on metal-support interfaces, J. Catal. 367 (2018) 194-205.

[33] F. Wang, C. Li, X. Zhang, M. Wei, D.G. Evans, X. Duan, Catalytic behavior of supported Ru nanoparticles on the {100}, {110}, and {111} facet of CeO$_2$, J. Catal. 329 (2015) 177-186.

[34] Y. Guo, S. Mei, K. Yuan, D.-J. Wang, H.-C. Liu, C.-H. Yan, Y.-W. Zhang, Low-temperature CO$_2$ methanation over CeO$_2$-Supported Ru single atoms, nanoclusters, and nanoparticles competitively tuned by strong metal-support interactions and H-spillover effect, ACS Catal. 8 (2018) 6203-6215.

[35] M. Tamura, S. Ishikawa, M. Betchaku, Y. Nakagawa, K. Tomishige, Selective hydrogenation of amides to alcohols in water solvent over a heterogeneous CeO$_2$-supported Ru catalyst, Chem. Commun. 54 (2018) 7503-7506.

[36] C.-J. Li, L. Chen, Organic chemistry in water, Chem. Soc. Rev. 35 (2006) 68-82.

[37] C.-R. Chang, Z.-Q. Huang, J. Li, The promotional role of water in heterogeneous catalysis: mechanism insights from computational modeling, WIREs Comput. Mol. Sci. 6 (2016) 679-693.

[38] P.H. Dixneuf, V. Cadierno, Metal-catalyzed reactions in water, Wiley-VCH, Weinheim, 2013.

[39] F. Joó, Aqueous biphasic hydrogenations, Acc. Chem. Res. 35 (2002) 738-745.

[40] M.-M. Wang, L. He, Y.-M. Liu, Y. Cao, H.-Y. He, K.-N. Fan, Gold supported on mesostructured ceria as an efficient catalyst for the chemoselective hydrogenation of carbonyl compounds in neat water, Green Chem. 13 (2011) 602.

[41] X. Xiang, W. He, L. Xie, F. Li, A mild solution chemistry method to synthesize hydrotalcite-supported platinum nanocrystals for selective hydrogenation of cinnamaldehyde in neat water, Catal. Sci. Technol. 3 (2013) 2819-2827.

[42] Z. Guo, Y. Chen, L. Li, X. Wang, G. L. Haller, Y. Yang, Carbon nanotube-supported Pt-based bimetallic catalysts prepared by a microwave-assisted polyol reduction method and their catalytic applications in the selective hydrogenation, J. Catal. 276 (2010) 314-326.

[43] J. Hidalgo-Carrillo, M.A. Aramendía, A. Marinas, J.M. Marinas, F.J. Urbano, Support and solvent effects on the liquid-phase chemoselective hydrogenation of crotonaldehyde over Pt catalysts, Appl. Catal. A-Gen. 385 (2010) 190-200.

[44] H. G. Manyar, D. Weber, H. Daly, J. M. Thompson, D. W. Rooney, L. F. Gladden, E. Hugh Stitt, J. Jose Delgado, S. Bernal, C. Hardacre, Deactivation and regeneration of ruthenium on silica in the liquid-phase hydrogenation of butan-2-one, J. Catal. 265 (2009) 80-88.

[45] S.-I. Fujita, Y. Sano, B. M. Bhanage, M. Arai, Supported liquid-phase catalysts

containing ruthenium complexes for selective hydrogenation of α,β-unsaturated aldehyde: importance of interfaces between liquid film, solvent, and support for the control of product selectivity, J. Catal. 225 (2004) 95-104.

[46] A. Rossin, L. Gonsalvi, A.D. Phillips, O. Maresca, A. Lledós, M. Peruzzini, Water-assisted H-H bond splitting mediated by [CpRu(PTA)$_2$Cl] (PTA=1,3,5-triaza-7-phosphaadamantane). A DFT analysis, Organomet. 26 (2007) 3289-3296.

[47] A. Rossin, G. Kovács, G. Ujaque, A. Lledós, F. Joó, The active role of the water solvent in the regioselective CO hydrogenation of unsaturated aldehydes by [RuH$_2$(mtppms)$_x$] in basic media, Organomet. 25 (2006) 5010-5023.

[48] J. Joubert, F. Delbecq, Understanding the selectivity in hydrogenation of α,β-unsaturated aldehydes: a water-assisted mechanism, Organomet. 25 (2006) 854-861.

[49] L.R. Merte, G. Peng, R. Bechstein, F. Rieboldt, C.A. Farberow, L.C. Grabow, W. Kudernatsch, S. Wendt, E. Laegsgaard, M. Mavrikakis, F. Besenbacher, Water-mediated proton hopping on an iron oxide surface, Science 336 (2012) 889-893.

[50] W.C. Conner, J.L. Falconer, Spillover in heterogeneous catalysis, Chem. Rev. 95 (1995) 759-788.

[51] Y. Dai, X. Gao, X. Chu, C. Jiang, Y. Yao, Z. Guo, C. Zhou, C. Wang, H. Wang, Y. Yang, On the role of water in selective hydrogenation of cinnamaldehyde to cinnamyl alcohol on PtFe catalysts, J. Catal. 364 (2018) 192-203.

[52] Y. Dai, X. P. Wu, Y. Tang, Y. Yang, X. Q. Gong, J. Fan, Selectivity switching resulting in the formation of benzene by surface carbonates on ceria in catalytic gas-phase oxidation of benzyl alcohol, Chem. Commun. 52 (2016) 2827-2830.

[53] V.V. Pushkarev, V.I. Kovalchuk, J.L. d'Itri, Probing defect sites on the CeO_2 surface with dioxygen, J. Phys. Chem. B 108 (2004) 5341-5348.

[54] Z. Wu, M. Li, J. Howe, H.M. Meyer III, S.H. Overbury, Probing defect sites on

CeO_2 nanocrystals with well-defined surface planes by Raman spectroscopy and O_2 adsorption, Langmuir 26 (2010) 16595-16606.

[55] X. Liu, Z. Wu, B. He, R. Yu, Structure and room-temperature ferromagnetism of Zn-doped SnO_2 nanorods prepared by solvothermal method, J. Phys. Chem. C 114 (2010) 4790-4796.

[56] Q. Zhao, D. Ju, X. Deng, J. Huang, B. Cao, X. Xu, Morphology-modulation of SnO_2 hierarchical architectures by Zn doping for glycol gas sensing and photocatalytic applications, Sci. Rep. 5 (2015) 7874-7882.

[57] V.O. Rodina, D.Y. Ermakov, A.A. Saraev, S.I. Reshetnikov, V.A. Yakovlev, Influence of reaction conditions and kinetic analysis of the selective hydrogenation of oleic acid toward fatty alcohols on Ru-Sn-B/Al_2O_3 in the flow reactor, Appl. Catal. B-Environ. 209 (2017) 611-620.

[58] M.A. Sánchez, V.A. Mazzieri, M.A. Vicerich, C.R. Vera, C.L. Pieck, Influence of the support material on the activity and selectivity of Ru-Sn-B catalysts for the selective hydrogenation of methyl oleate, Ind. Eng. Chem. Res. 54 (2015) 6845-6854.

[59] V.M. Deshpande, W.R. Patterson, C.S. Narasimhan, Studies on ruthenium-tin boride catalysts I. Characterization, J. Catal. 121 (1990) 165-173.

[60] F. Wang, C. Li, X. Zhang, M. Wei, D.G. Evans, X. Duan, Catalytic behavior of supported Ru nanoparticles on the {100}, {110}, and {111} facet of CeO_2, J. Catal. 329 (2015) 177-186.

[61] S.Y. Chin, C.T. Williams, M.D. Amiridis, FTIR Studies of CO adsorption on Al_2O_3- and SiO_2-supported Ru catalysts, J. Phys. Chem. B 110 (2006) 871-882.

[62] B.T. Loveless, C. Buda, M. Neurock, E. Iglesia, CO Chemisorption and dissociation at high coverages during CO hydrogenation on Ru catalysts, J. Am. Chem. Soc. 135 (2013) 6107-6121.

[63] B.A. Riguetto, J.M.C. Bueno, L. Petrov, C.M.P. Marques, An infrared study of CO adsorption on silica-supported Ru-Sn catalysts, Spectrochim. Acta. A-Mol. Biomol. Spectrosc. 59 (2003) 2141-2150.

[64] M.A. Sánchez, Y. Pouilloux, V.A. Mazzieri, C.L. Pieck, Influence of the operating conditions and kinetic analysis of the selective hydrogenation of oleic acid on Ru-Sn-B/Al_2O_3 catalysts, Appl. Catal. A-Gen. 467 (2013) 552-558.

[65] M.A. Sánchez, V.A. Mazzieri, M.R. Sad, R. Grau, C.L. Pieck, Influence of preparation method and boron addition on themetal function properties of Ru-Sn catalysts for selective carbonyl hydrogenation, J. Chem. Technol. Biotechnol. 86 (2011) 447-453.

[66] B.A. Riguetto, C.E.C. Rodrigues, M.A. Morales, E. Baggio-Saitovitch, L. Gengembre, E. Payen, C.M.P. Marques, J.M.C. Bueno, Ru-Sn catalysts for selective hydrogenation of crotonaldehyde: effect of the Sn/(Ru+Sn) ratio, Appl. Catal. A-Gen. 318 (2007) 70-78.

[67] S.G. Wettstein, J.Q. Bond, D.M. Alonso, H.N. Pham, A.K. Datye, J.A. Dumesic, RuSn bimetallic catalysts for selective hydrogenation of levulinic acid to γ-valerolactone, Appl. Catal. B-Environ. 117-118 (2012) 321-329.

[68] A.M. Silva, M.J. Mendes, E. Jordão, M.A. Fraga, Hydrogenation of citral over ruthenium-tin catalysts, Appl. Catal. A-Gen. 241 (2003) 155-165.

[69] V.M. Deshpande, K. Ramnarayan, C.S. Narasimhan, Studies on ruthenium-tin boride catalysts II. Hydrogenation of fatty acid esters to fatty alcohols, J. Catal. 121 (1990) 174-182.

[70] H. Rojas, G. Borda, J.J. Martínez, J. Valencia, P. Reyes, Liquid phase hydrogenation of citral and intermediaries over Ir/TiO_2/SiO_2 catalysts: kinetic study, J. Mol. Catal. A-Chem. 286 (2008) 70-78.

[71] U.K. Singh, M.A. Vannice, Liquid-phase hydrogenation of citral over Pt/SiO_2 catalysts: I. Temperature effects on activity and selectivity, J. Catal. 191 (2000) 165-180.

[72] I. Bergault, P. Fouilloux, C. Joly-Vuillemin, H. Delmas, Kinetics and intraparticle diffusion modelling of a complex multistep reaction: hydrogenation of acetophenone over a rhodium catalyst, J. Catal. 175 (1998) 328-337.

[73] J.P. Breen, R. Burch, J. Gomez-Lopez, K. Griffin, M. Hayes, Steric effects in the selective hydrogenation of cinnamaldehyde to cinnamyl alcohol using an Ir/C catalyst, Appl. Catal. A-Gen. 268 (2004) 267-274.

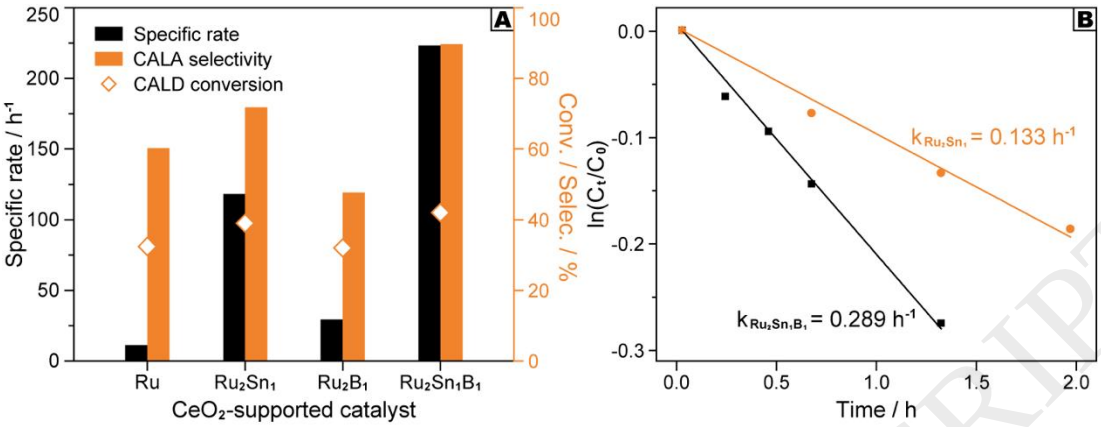

Fig.1. (A) The catalytic performances of CeO_2-supported Ru catalysts in hydrogenation of cinnamaldehyde (CALD) to cinnamyl alcohol (CALA) in water solvent. The reaction conditions: 20-55 mg of catalyst, 200 µL of CALD, 10 mL of water, 20 bar of H_2, 60 ^oC, and 2-12 h of time duration to reach similar CALD conversions at approximately 40%. (B) The reaction rate constants (*k*) of $Ru_2Sn_1B_1/CeO_2$ and Ru_2Sn_1/CeO_2 catalysts under identical conditions.

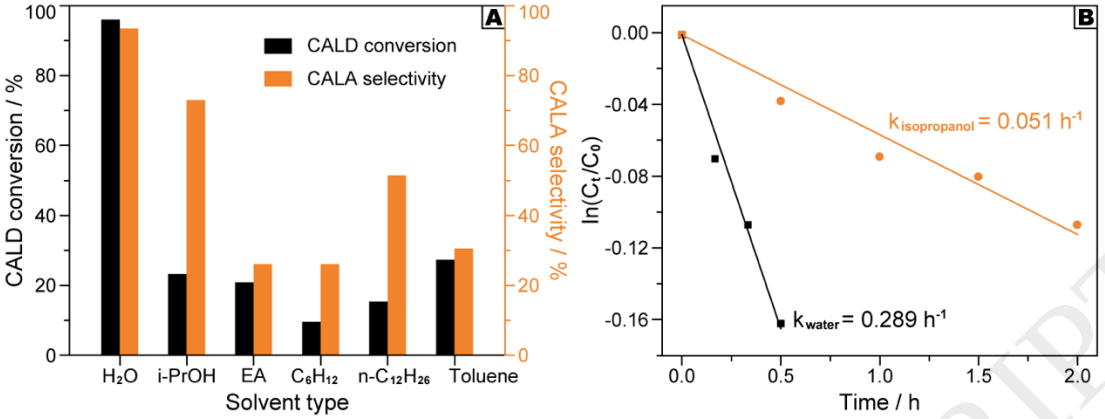

Fig. 2. (A) The catalytic hydrogenation performance of $Ru_2Sn_1B_1/CeO_2$ catalyst in various solvents. The reaction conditions: 20 mg of catalyst, 200 μL of CALD, 10 mL of solvent (i-PrOH, EA, C_6H_{12} and n-$C_{12}H_{26}$ referred to isopropanol, ethyl acetate, cyclohexane and n-dodecane, respectively), 20 bar of H_2, 100 °C, 4 h. (B) The reaction rate constants (*k*) of $Ru_2Sn_1B_1/CeO_2$-catalyzed CALD hydrogenation with isopropanol or water as solvent.

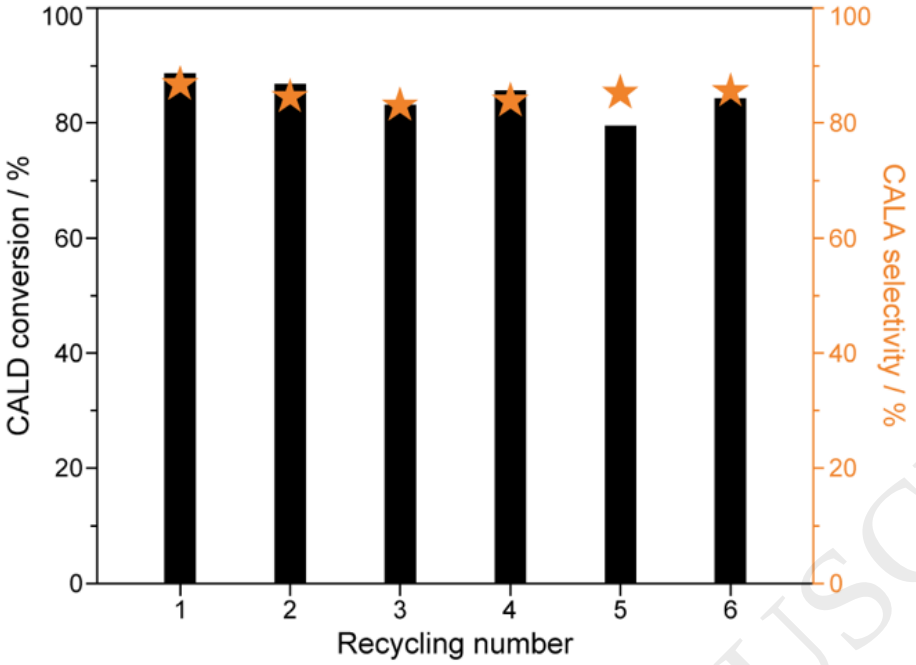

Fig. 3. Recycling stability of the $Ru_2Sn_1B_1/CeO_2$ catalyst in the selective hydrogenation of CALD in water as the solvent. Reaction conditions: 20 mg of catalyst, 200 μL of CALD, 10 mL of H_2O, 20 bar of H_2, 100 °C, 4 h.

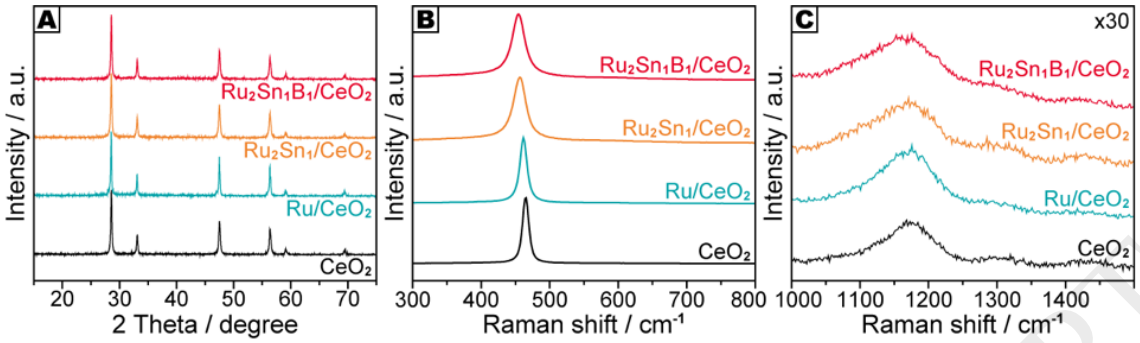

Fig. 4. XRD patterns (A) and Raman spectra (B-C) of different catalysts.

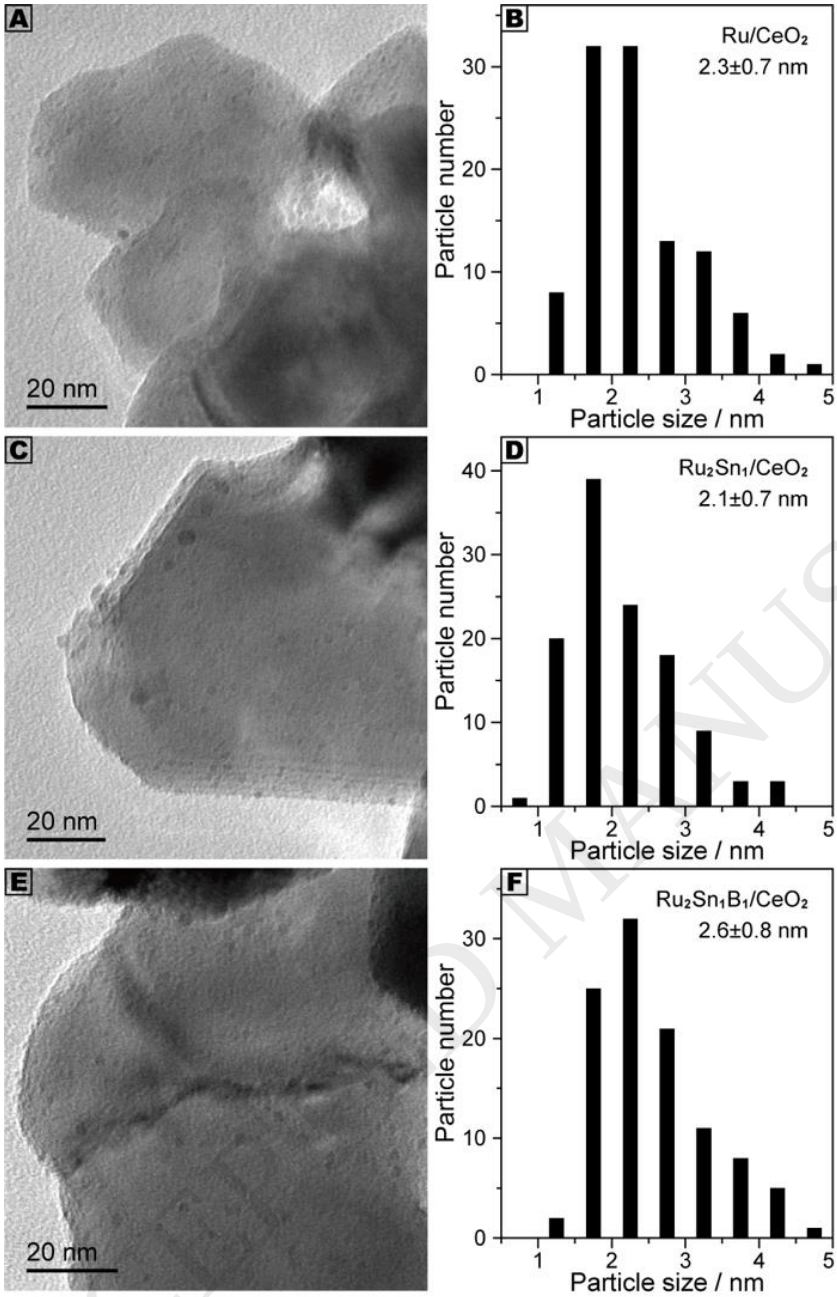

Fig. 5. TEM images and distributions of average particle sizes for Ru/CeO_2, Ru_2Sn_1/CeO_2 and $Ru_2Sn_1B_1/CeO_2$ catalysts.

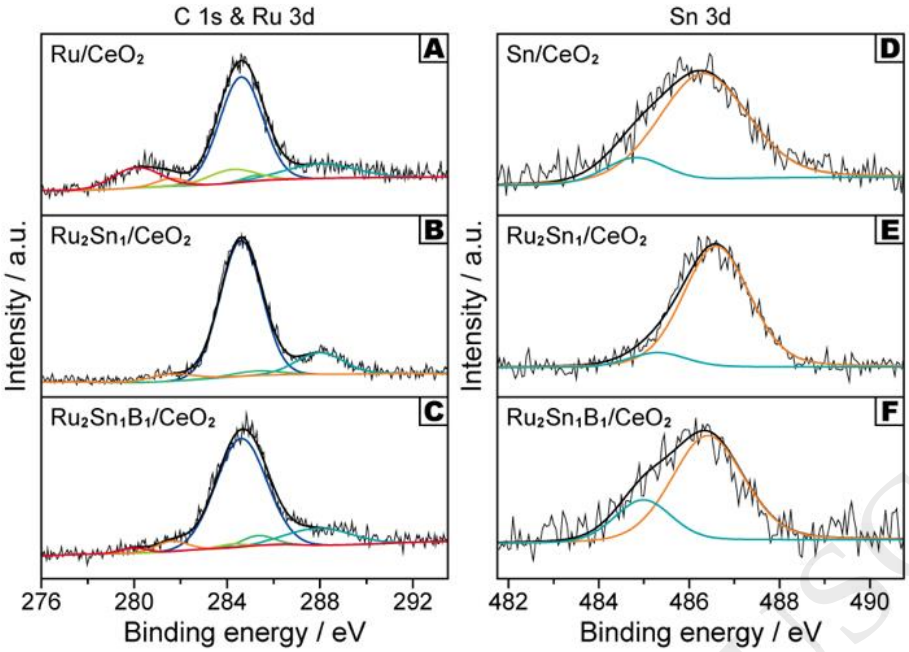

Fig. 6. XPS spectra of Ru 3d and Sn 3d core levels for CeO_2-supported Ru catalysts.

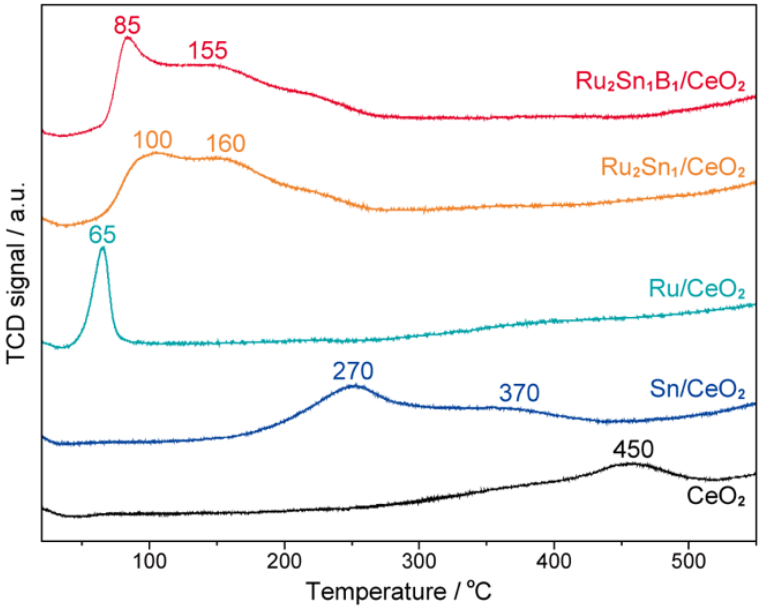

Fig. 7. H_2-TPR curves of various catalysts.

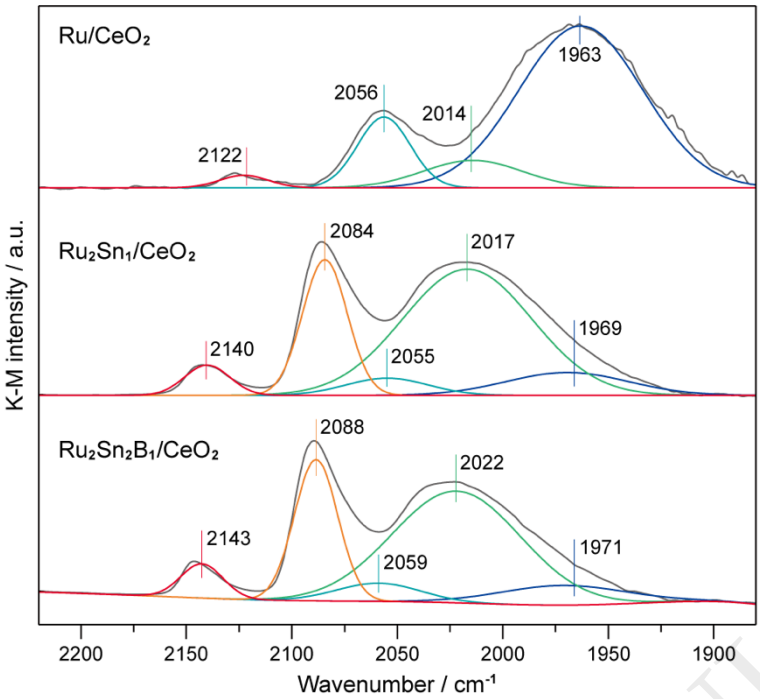

Fig. 8. Room-temperature CO-adsorption DRIFTs spectra of CeO_2-supported Ru-based catalysts.

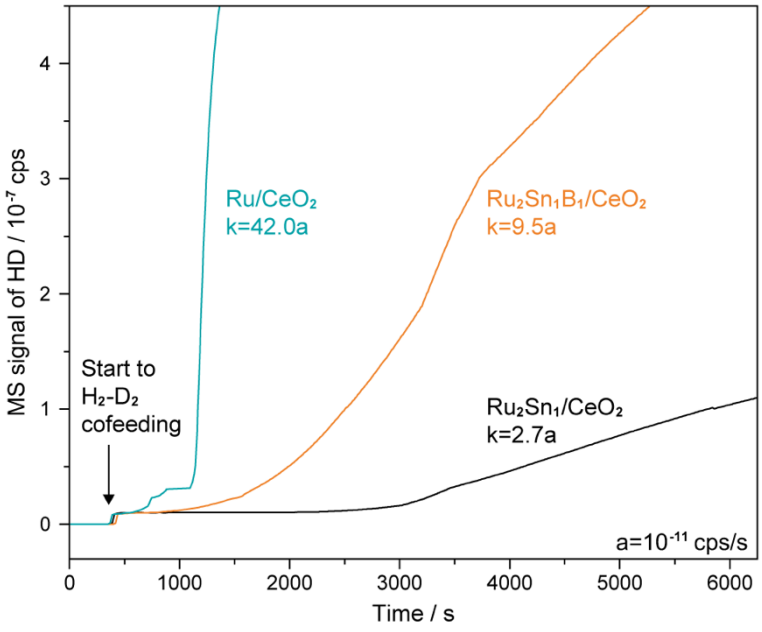

Fig. 9. MS signals of generated HD product in the H_2-D_2 exchange experiments on CeO_2-supported Ru, Ru_2Sn_1 and $Ru_2Sn_1B_1$ catalysts.

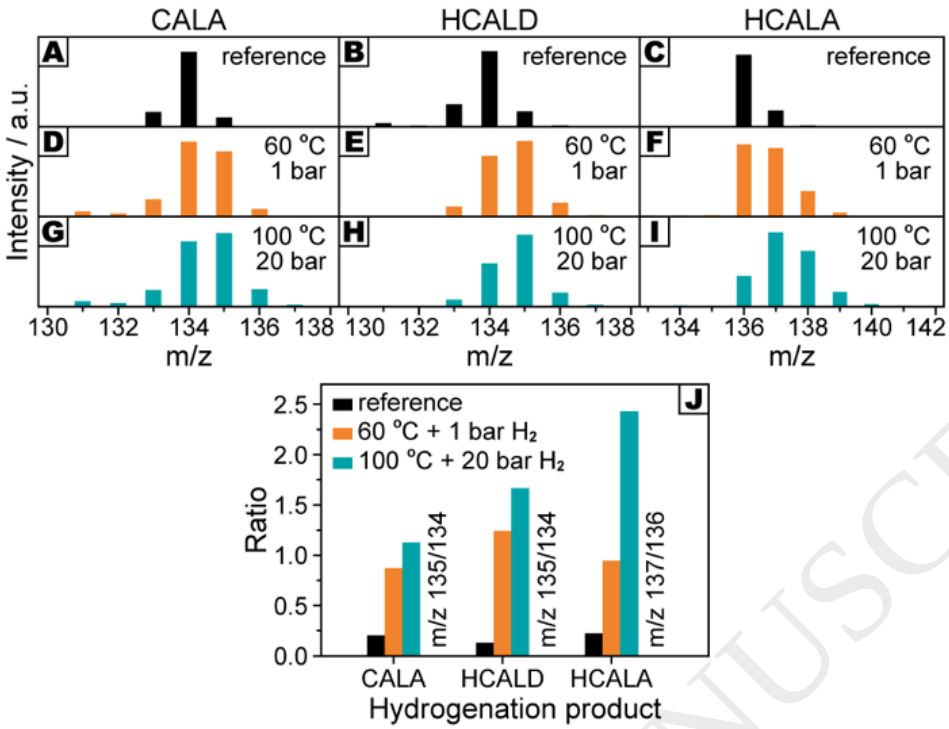

Fig. 10. MS spectra of hydrogenation products in D_2O-labeling reaction experiments (A-C) Reference experiments without catalyst, (D-I) $Ru_2Sn_1B_1/CeO_2$-catalyzed reactions and (J) summarized results of deuteration degrees.

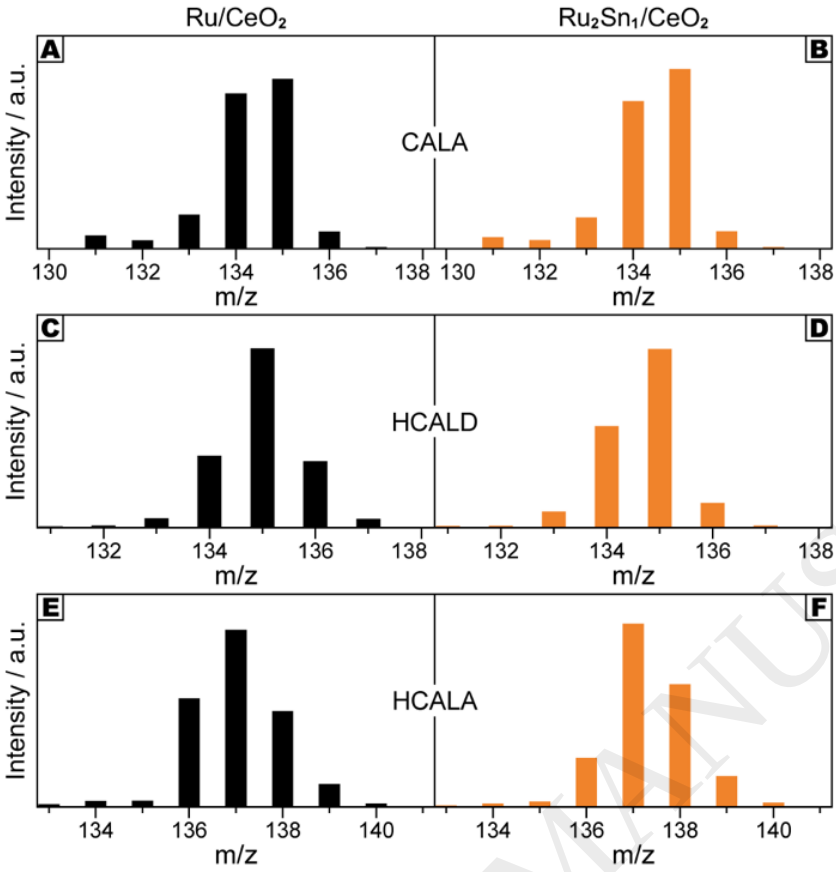

Fig. 11. MS spectra of three main products in CALD hydrogenation reactions over Ru/CeO_2 and Ru_2Sn_1/CeO_2 catalysts.

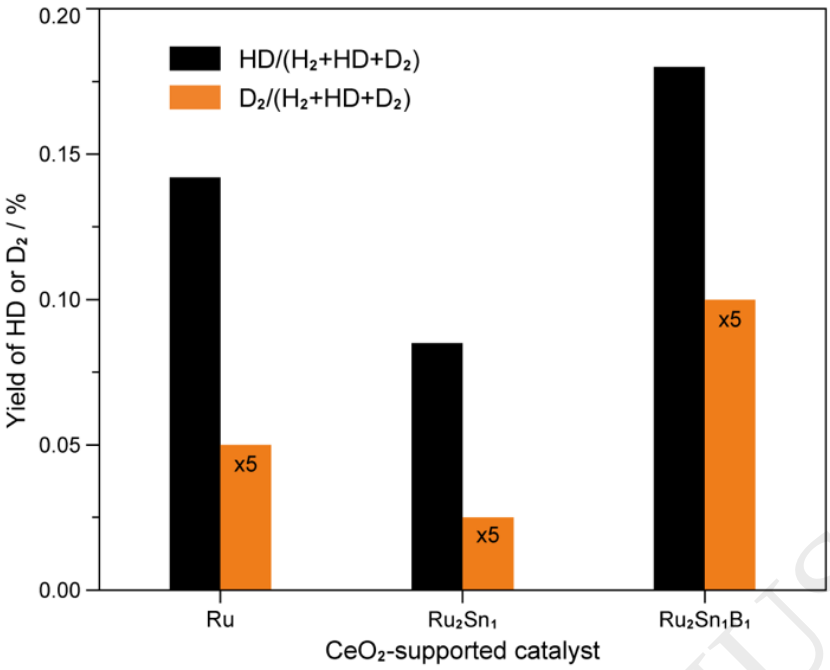

Fig. 12. Yields of generated gaseous HD and D_2 products in the H_2-D_2O exchange experiments on CeO_2-supported Ru, Ru_2Sn_1 and $Ru_2Sn_1B_1$ catalysts.

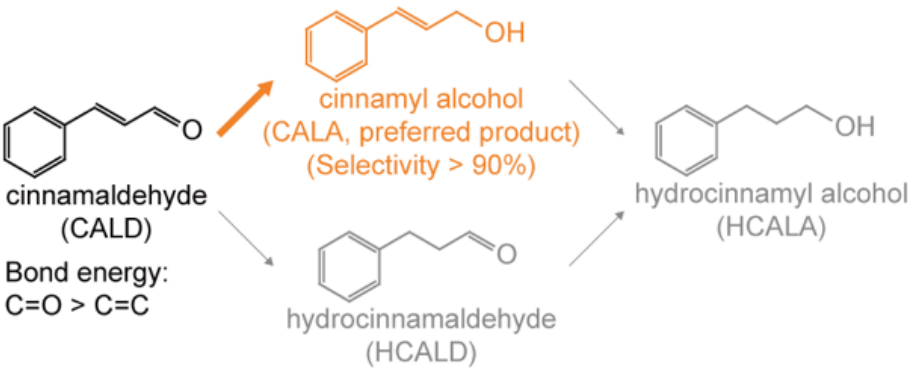

Scheme 1. Reaction network of RuSnB/CeO_2-catalyzed CALD hydrogenation.

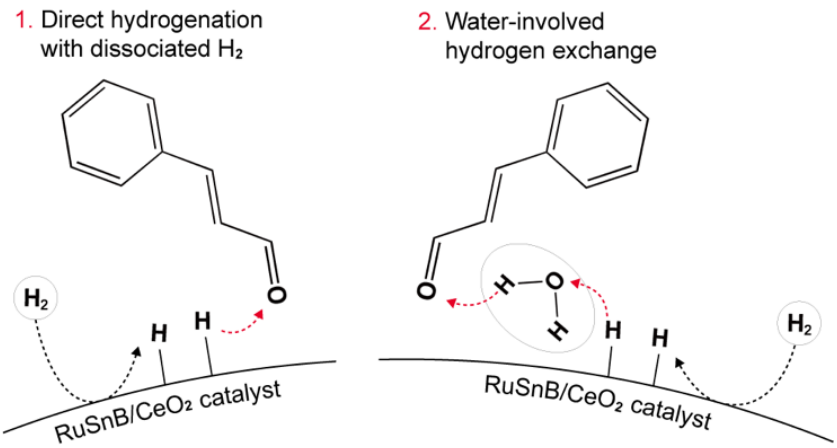

Scheme 2. The schematic diagram of two possible reaction pathways in RuSnB/CeO_2-catalyzed CALD hydrogenation.

Table 1. Structural information of various CeO_2-supported Ru catalysts.

Catalyst	Ru[a] (wt.%)	Sn[a] (wt.%)	B[a] (wt.%)	BET area[b] (m^2/g)	NPs size[c] (nm)	Surface Ru species[d] (at.%)		Surface Sn species[d] (at.%)	
						Ru^0	$Ru^{\delta+}$	Sn^0	$Sn^{2+/4+}$
Ru/CeO_2	0.67	/	/	22.7	2.3±0.7	80	20	/	/
Ru_2Sn_1/CeO_2	0.75	0.35	/	19.3	2.1±0.7	0	100	10	90
$Ru_2Sn_1B_1/CeO_2$	0.77	0.32	0.04	24.7	2.6±0.8	26	74	24	76

[a] Loading amounts of Ru, Sn and B were calculated from ICP-OES measurement results.

[b] BET specific surface areas were obtained from nitrogen adsorption isotherms.

[c] Average NPs (nanoparticles) sizes were analyzed from TEM images.

[d] Relative ratios of surface Ru and Sn species were obtained from XPS spectra of Ru 3d and Sn 3d orbits.

Table 2. Characteristic frequencies and peak areas of DRIFT spectral features observed following the room temperature adsorption of CO on Ru-based catalysts.

Catalyst	Peak	1[a]	2[b]	3[c]	4[d]	5[e]	$Ru^{\delta+}/Ru^0$
Ru/CeO_2	Frequency (cm^{-1})	1963	2014	2056	/	2122	12.3/87.7
	Relative area (%)	74.0	10.1	13.7	/	2.2	
Ru_2Sn_1/CeO_2	Frequency (cm^{-1})	1969	2017	2055	2084	2140	84.9/15.1
	Relative area (%)	10.0	58.3	5.1	21.7	4.9	
$Ru_2Sn_1B_1/CeO_2$	Frequency (cm^{-1})	1971	2022	2059	2088	2143	84.6/15.4
	Relative area (%)	9.5	55.4	5.9	23.7	5.5	

[a] Bridge-bonded CO, $[Ru_2\text{-}(CO)]$.

[b] Dicarbonyl CO species on Ru^{2+}, $[Ru^{2+}\text{-}(CO)_2]$.

[c] Dicarbonyl CO species on Ru^0, $[Ru^0\text{-}(CO)_2]$.

[d] CO species adsorbed on $Ru^{\delta+}$ sites, including dicarbonyl, tricarbonyl and linear adsorption models, $[Ru^{\delta+}\text{-}(CO)_x$, δ=1-3, x=1-3].

[e] Tricarbonyl CO species on $Ru^{\delta+}$, $[Ru^{\delta+}\text{-}(CO)_3$, δ=1-3].